Photodeposited metal-semiconductor nanocomposites and their applications

Yoonkyung Lee [a, 1], Eunpa Kim [b, 1], Yunjeong Park [a], Jangho Kim [c], WonHyoung Ryu [d], Junsuk Rho [e, f, **], Kyunghoon Kim [a, *]

[a] School of Mechanical Engineering, Sungkyunkwan University, Suwon 16419, Republic of Korea
[b] Semiconductor R&D Center, Samsung Electronics, Hwaseong 18448, Republic of Korea
[c] Department of Rural and Biosystems Engineering, Chonnam National University, Gwangju 61186, Republic of Korea
[d] Department of Mechanical Engineering, Yonsei University, Seoul 03722, Republic of Korea
[e] Department of Mechanical Engineering, Pohang University of Science and Technology (POSTECH), Pohang 37673, Republic of Korea
[f] Department of Chemical Engineering, Pohang University of Science and Technology (POSTECH), Pohang 37673, Republic of Korea

ARTICLE INFO

ABSTRACT

While two-dimensional layered nanomaterials including transition metal oxides and transition metal dichalcogenides have been widely researched because of their unique electronic and optical properties, they still have some limitations. To overcome these limitations, transition metal oxides and transition metal dichalcogenides based nanocomposites have been developed using various methods and have exhibited superior properties. In this paper, we introduce the photodeposition method and review the photodeposition of metal nanoparticles on the surface of transition metal oxide and transition metal dichalcogenides. Their current applications are also explained, such as photocatalysis, hydrogen evolution reaction, surface enhanced Ramanscattering, etc. This approach for nanocomposites has potential for future research areas such as photocatalysis, hydrogen evolution reaction, surface enhanced Raman scattering, and other applications. This approach for nanocomposite has the potential for future research areas.

© 2018 The Chinese Ceramic Society. Production and hosting by Elsevier B.V. This is an open access article under the CC BY-NC-ND license (http://creativecommons.org/licenses/by-nc-nd/4.0/).

Contents

* Corresponding author. Department of Mechanical Engineering, Pohang University of Science and Technology (POSTECH), Pohang 37673, Republic of Korea.
** Corresponding author. School of Mechanical Engineering, Sungkyunkwan University, Suwon 16419, Republic of Korea.
E-mail addresses: yi9257kr@skku.edu (Y. Lee), eunpa.kim@samsung.com (E. Kim), djy828@skku.edu (Y. Park), rain2000@jnu.ac.kr (J. Kim), whryu@yonsei.ac.kr (W. Ryu), jsrho@postech.ac.kr (J. Rho), kenkim@skku.edu (K. Kim).
Peer review under responsibility of The Chinese Ceramic Society.
[1] These authors contributed equally to this work.

1. Introduction

Recently, due to advances in nanotechnology, nanomaterials have attracted considerable attention due to their unique properties such as high aspect ratio [1–8]. In recent years, nanocomposite materials have been widely studied since they have advantages of their individual constituent materials and sometimes exhibit better properties than their individuals [9–22]. Consequently, developing nanocomposites could be a solution to adjust the properties of individual nanomaterials appropriately. In particular, in the field of semiconductor materials, nanocomposites composed of two or more materials are widely used to alter their electronic and optical properties [16,17,19,22,23]. Usually, semiconductor materials are decorated with noble metal nanoparticles and these nanocomposites are prevalently used for field-effect transistors [24–26], photodetectors [27], and photocatalysts [28–32].

Over the past few decades, transition metal oxides (TMOs) have been studied and developed for diverse applications [33–37]. Recently, transition metal dichalcogenides (TMDs) have also received considerable attention as an analogue of graphene due to their two-dimensional (2D) layered structural similarity [38–43]. While these TMO and TMD materials have unconventional electronic and optical properties, they need to be properly tuned for specific applications. Various methods have been developed to change their properties, such as forming nanocomposites by the combination of other nanomaterials. For example, TiO_2, one of the most developed TMOs, has been studied as a photocatalyst; however, it can only absorb UV light due to its very large band gap of $3.0-3.2$ eV, which decreases the efficiency for photocatalysis [19,44]. To overcome this weakness, TiO_2 incorporated with metal nanoparticles has been studied, whereby the metal nanoparticles enhance the catalytic properties of TiO_2 since they tune the Fermi level of TiO_2 and act as an electron sink [37].

Until now, noble metal/semiconductor nanocomposites has been synthesized via various methods such as hydrothermal [28,45–48], droplet [24,49], electrochemical [50,51], and thermal evaporation [25–27] etc. [52–56]. The photodeposition method is one of the easiest methods to synthesize noble metal/semiconductor nanocomposites by utilizing the band gap of the semiconductor. Compared with most other methods that need a high temperature, an additional redox agent, electric potential, or multistep processing, the photo-induced reduction method requires only the irradiation of a light source. Furthermore, with the photodeposition of noble nanoparticles over 2D substrates, it is easy to control the size of noble metal nanoparticles by adjusting the concentration of the metal precursor, irradiating time, and irradiating power. Also, this method enables material selectivity, whereby noble metal nanoparticles are only deposited on the semiconductor templates [57,58].

In this paper, we review the recent progress and applications of TMO and TMD based nanocomposites decorated with noble metal nanoparticles prepared by photodeposition method. First, the basic principle of the photodeposition method is introduced and several applications of nanocomposites are then discussed, such as photocatalysis, hydrogen evolution reaction (HER), surface enhanced Raman scattering (SERS), etc. TMO and TMD have two main roles: (i) templates offering the sites for metal nanoparticles and (ii) photocatalyst for photodeposition method. Noble metal nanoparticles contribute to the enhancement of application performance by providing (i) active sites for reaction and (ii) electron acceptors.

2. Principle of photodeposition method

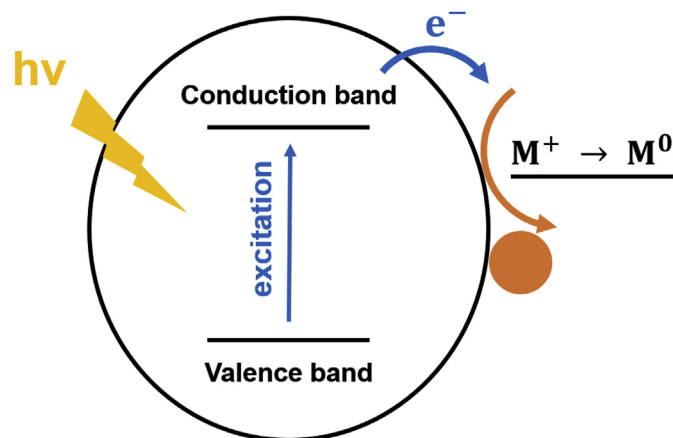The photodeposition method is based on the photocatalytic

Fig. 1. Schematic diagram of photodeposition method. When light is absorbed in the band gap, electrons from valence band are excited and migrate to reduce metal ions to metal. hv, light energy; e^-, photoexcited electron; M^+, metal ion; M^0, metal.

property of semiconductor materials afforded by their band gap. Several conditions are needed to enable the photodeposition method. First, the photon energy of the exposure light should be larger than the energy band gap of the semiconductor. When light that has the proper energy level for the band gap of the semiconductor is absorbed, electrons from the valence band can be excited. Second, the reduction potential of the metal ion should be more positive than the conduction band energy level of the semiconductor. Third, the efficient separation and migration of photogenerated electron-hole pairs is necessary. Finally, the semiconductor should act as a template for active sites of metal deposition and have a large surface area, as shown in Fig. 1. If these four conditions are met, the synthesis of metal/semiconductor nanocomposite by photodeposition method is possible, since nanoscale semiconductor materials have many active sites that have large surface energy due to their morphology. Also, this is a simple and green method since it does not require the addition of chemical reagents or any conditions other than light exposure.

3. Applications

3.1. Photocatalyst

Photocatalysis is one of the most efficient ways to convert solar energy into chemical or electrical energy, and has been researched for a long time to develop high efficient photocatalysts [43,59]. Semiconductor nanomaterials show unique properties compared to their bulk counterparts; for example, their electrical properties are easily controlled by changing their size or dimensions [19,60]. However, individual semiconductor nanomaterials have limitations whereby the migration of photo-generated electron-hole pairs is difficult and they have low photocatalysis efficiency. To overcome these limitations, noble metal/semiconductor nanocomposites can be a solution to enhance photocatalysis efficiency. In this section, we describe TMO based metal nanocomposite photocatalysts synthesized by photodeposition method.

In a study by Yu et al. [61], the photodeposition of Pt nanoparticles on TiO_2 nanosheets was conducted under a 350 W Xe lamp for 20 min. They used H_2PtCl_6 solution as a metal precursor with different concentrations ranging from 0, 0.06, 0.13, 0.26, 0.35, to 0.78 mM. After the photodeposition process, they collected sediment by centrifugation and then rinsed the sediment with distilled water and ethanol three times. The final products were

dried at 80 °C for 12 h, and the nominal weight ratios of Pt to Ti were 0, 0.5, 1, 2, 4, and 6 wt%, respectively. After the preparation of Pt/TiO$_2$ nanocomposites, they investigated the photocatalytic activities of water splitting for H$_2$ production under a 350 W Xe lamp. The highest photocatalytic activity of H$_2$ production was obtained with the nominal weight ratio of Pt to Ti of 2 wt%. This enhancement of photocatalytic reaction is based on the role of Pt nanoparticles. During the reaction, electrons are trapped by the Pt nanoparticles, and this decreases the recombination of photoexcited electron-hole pairs, thus increasing the H$_2$ production. Similarly, Li et al. [62] studied Pt/TiO$_2$ porous nanosheets for the photocatalystic reduction of CO$_2$ to methane. Pt nanoparticles were deposited on the surface of TiO$_2$ by reducing H$_2$PtCl$_6$ ethanol solution under UV irradiation for 1 h. The size of the Pt nanoparticles was 3–4 nm and they were uniformly deposited on the TiO$_2$ nanosheets. Characterization of the optical properties was conducted by measuring the UV–vis absorbance spectra of TiO$_2$ and Pt/TiO$_2$. The absorbance peak was broadened to around 350–550 nm after Pt deposition due to the surface plasmon resonance of Pt nanoparticles; however, the absorbance intensity in the UV range decreased because of the shield effect of the Pt nanoparticles. They then measured the photocatalytic reduction rate of CO$_2$ to methane on TiO$_2$ and Pt/TiO$_2$. The result showed that Pt/TiO$_2$ exhibited a significantly higher photoreduction rate of 20.51 ppm/h·cm^2 than that of TiO$_2$ of 3.71 ppm/h·cm^2. This occurs because the

photoexcited electrons are trapped by Pt nanoparticles which have a lower Fermi level and they can then easily transfer to reduce CO$_2$ to methane. Lv et al. [63] prepared Pt modified TiO$_2$ nanotube arrays (TiO$_2$ NTAs) and demonstrated their visible light photocatalytic performance. They deposited Pt nanoparticles on the TiO$_2$ NTAs, reducing the different concentrations of the H$_2$PtCl$_6$ solution (1, 2, 3, and 4 mM) under a 500 W mercury lamp for 30 min. The samples were labeled as 1 Pt/TiO$_2$, 2 Pt/TiO$_2$, 3 Pt/TiO$_2$, and 4 Pt/TiO$_2$. Fig. 2(a)-(e) show the HRTEM images of 3 Pt/TiO$_2$ morphology and the EDX mapping of Ti, O, and Pt, which clearly show that the Pt nanoparticles are uniformly deposited on the TiO$_2$ NTAs. Fig. 2(f) shows the UV–vis absorbance spectra of TiO$_2$ NTAs and Pt/TiO$_2$ NTAs, indicating that the deposition of Pt enhances the absorbance of Pt/TiO$_2$ NTAs of an overall visible range of light (400–800 nm). The highest visible light absorption is shown in 3 Pt/TiO$_2$. Fig. 2(g) shows the photodegradation rate of methyl orange under visible light irradiation with different photocatalysts. It is demonstrated that the TiO$_2$ NTAs show a photodegradation rate of 2% after 2 h of irradiation, whereas the photodegradation rate of all the Pt/TiO$_2$ NTAs after Pt deposition increases and the highest photodegradation rate of 84.27% is observed after 2 h of irradiation at 3 Pt/TiO$_2$ NTAs, consistent with the UV–vis absorbance spectra. As shown in Fig. 2(h), the visible-light-driven photocatalysis mechanism involves the migration of the photoexcited electron due to surface plasmon resonance of the Pt nanoparticles to TiO$_2$ followed
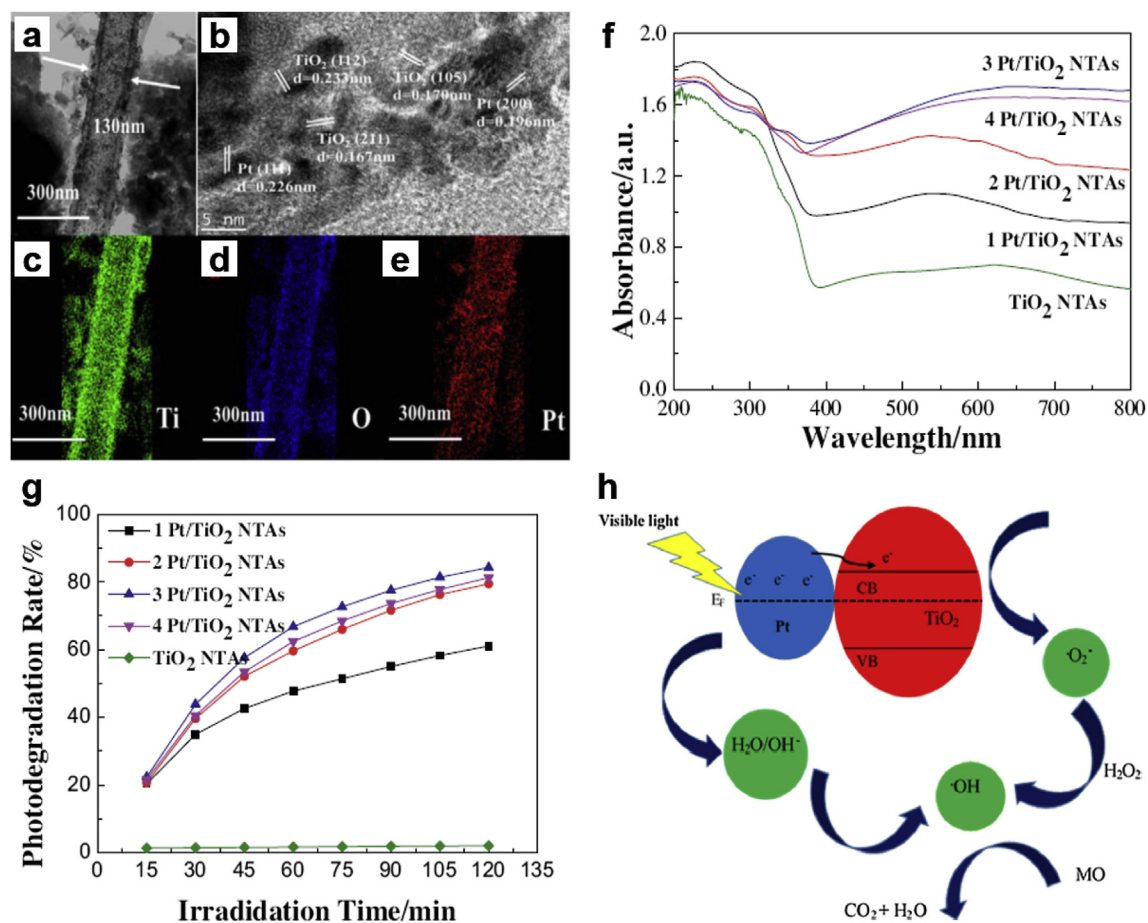

Fig. 2. (a) and (b) HRTEM images of Pt/TiO$_2$ NTAs. EDX mappings of (c) Ti (d) O (e) Pt. (f) UV–vis absorbance spectra of pure TiO$_2$ NTAs and different amounts of Pt/TiO$_2$ NTAs. (g) Photodegradation rate vs. visible light irradiation time. (h) Schematic diagram of the photocatalysis [63].

by the occurrence of redox reaction.

Leong et al. [64] demonstrated visible-light-driven photo-catalytic activity of Pd/TiO$_2$ nanocomposites. Pd/TiO$_2$ nano-composites were synthesized by photodeposition method under sunlight at an intensity between 150 and 180 W m^{-2}. Na$_2$PdCl$_4$ was used as a metal precursor at different amounts (0.5 wt%, 1.0 wt%, and 3.0 wt%) to investigate the effect of the amount of Pd nano-particle. As shown in Fig. 3(a)-(c), Pd nanoparticles were formed on the surface of TiO$_2$ and the morphology of TiO$_2$ was not affected by the formation of the Pd nanoparticles. Fig. 3(d) shows the optical absorbance spectra of TiO$_2$ and Pd/TiO$_2$ with different amounts of Pd nanoparticles. Fig. 3(e) shows the photoluminescence (PL)

spectra which indicate the recombination rate of photogenerated electron-hole pairs. It is clearly shown that the Pd nanoparticles contributed to increasing of absorbance in the visible range due to surface plasmon absorbance, and 1.0 wt% Pd/TiO$_2$ exhibited the largest optical absorption and the lowest PL emission. The PL peak of Pd/TiO$_2$ was considerably decreased compared to TiO$_2$, which definitely demonstrates that Pd nanoparticles enhanced electron transfer or electron trapping. The photocatalytic activities of Pd/TiO$_2$ were also verified by measuring the photodegradation of amoxicillin (AMX) under a 500 W tungsten-halogen lamp with a high pass UV light filter as a visible light source. As shown in Fig. 3(f) and (g), 0.5 wt% Pd/TiO$_2$ exhibited the best photocatalytic
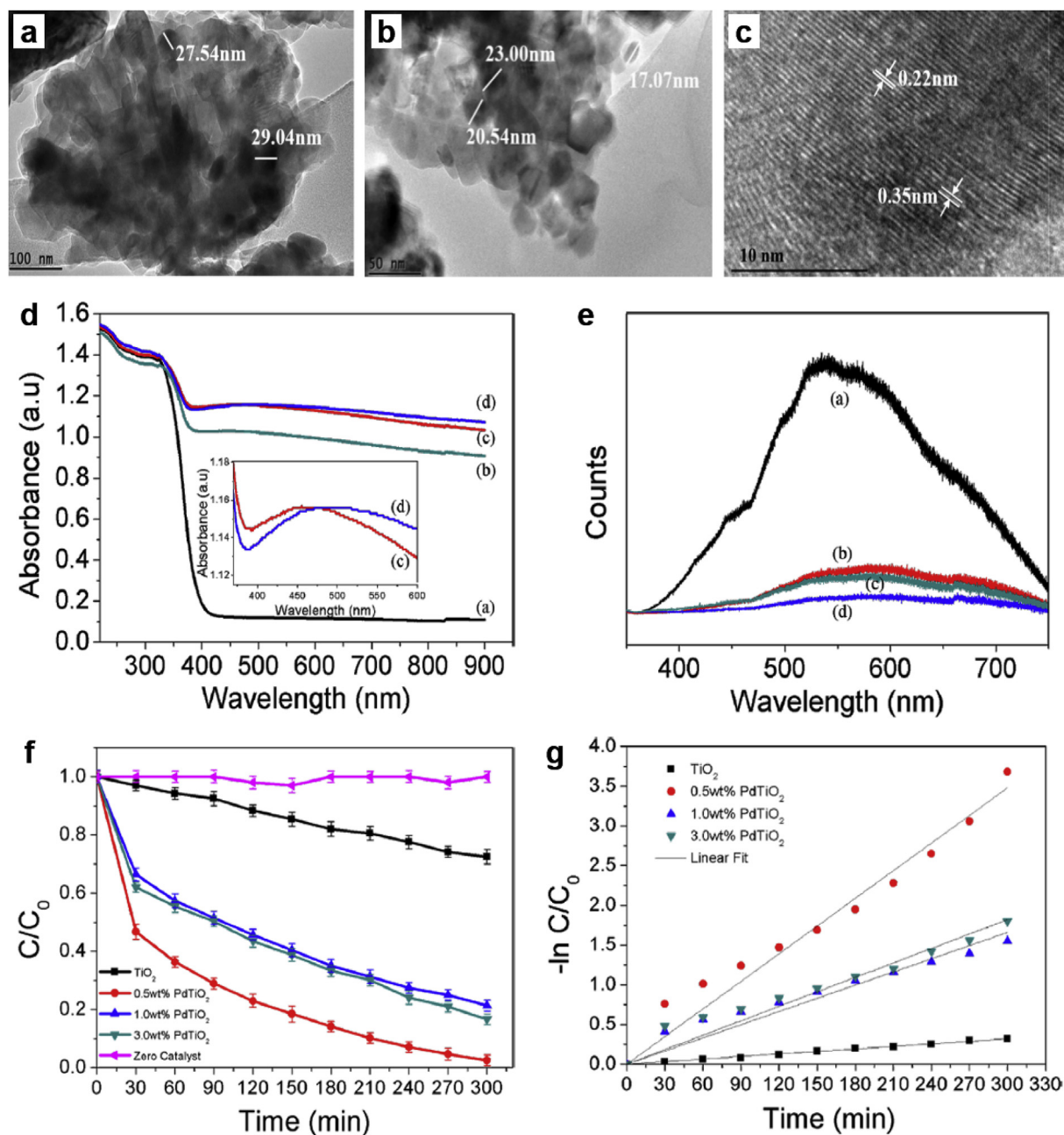

Fig. 3. (a)–(c) HRTEM images of Pd/TiO$_2$ with 0.5 wt%. (d) UV−vis absorbance spectra of a) TiO$_2$, b) 3.0 wt% Pd/TiO$_2$, c) 0.5 wt% Pd/TiO$_2$ and d) 1.0 wt% Pd/TiO$_2$. (e) Photo-luminescence spectra of a) TiO$_2$, b) 0.5 wt% Pd/TiO$_2$, c) 3.0 wt% Pd/TiO$_2$ and d) 1.0 wt% Pd/TiO$_2$. (f) and (g) Photocatalytic degradation of AMX [64].

efficiency, which did not correspond to the optical spectrum results. This result is attributed to the increase in the number of Pd nanoparticles that can block the light, thus the absorbance is decreased and photogenerated electrons are thus reduced. Khojasteh et al. [65] also carried out a similar study on the Pd/TiO$_2$ photocatalyst and compared the Pd/TiO$_2$ photocatalyst with TiO$_2$ and PdO/TiO$_2$. TiO$_2$, PdO/TiO$_2$, and Pd/TiO$_2$ were prepared by sol-gel, sol-gel-hydrothermal, and photodeposition method, respectively. In the photodeposition method, Pd(NO$_3$)$_2$·2H$_2$O was reduced on the surface of TiO$_2$ under UV irradiation for 10 h. Optical absorbance was measured by UV–vis spectroscopy, showing that Pd/TiO$_2$ improved the absorbance of the UV range since Pd nanoparticles reduce the band gap of TiO$_2$. Corresponding to the optical absorbance result, Pd/TiO$_2$ exhibited the most efficient photodegradation of Rhodamine B under UV irradiation since Pd particles act as electron acceptors which can decrease the recombination of photogenerated electron-hole pairs, similar to a study by Leong et al. [64].

For other TMO materials, Wang et al. [66] synthesized Au nanoparticles sensitized ZnO nanopencil arrays which enhanced the photoelectrochemical properties of water splitting for H$_2$ production. Au nanoparticles were deposited on the ZnO nanopencil by the photodeposition method. The aqueous solution of HAuCl$_4$ was used as a metal precursor and the photodeposition process was conducted under a 300 W Xe lamp irradiation for 1 min with an intensity of 5 mW cm^{-2}. Photoelectrochemical properties were measured using the three-electrode system under a 300 W Xe lamp with an intensity of 100 mW cm^{-2}. The photocurrent density of Au/

ZnO nanopencils was higher than that of ZnO nanopencils. In this reaction, Au nanoparticles generated hot electrons by plasmon-induced irradiation. These hot electrons transferred to the conduction band of ZnO and enhanced photocurrent intensity. Also, a wider range of optical absorbance was observed in the Au/ZnO nanopencils compared to the ZnO nanopencils due to the surface plasmon resonance effect of the Au nanoparticles.

3.2. Hydrogen evolution reaction (HER)

Although hydrogen is an attractive energy, it does not exist in free form, and mostly exists as a component in water and hydrocarbons [67]. Thus, considerable research has been carried out to find a way to extract hydrogen from compounds via hydrogen evolution reaction (HER) [68–71].

Chen et al. [72] investigated the photocatalytic reaction of Au/TiO$_2$ for hydrogen evolution by water splitting. They mixed TiO$_2$ powder and 0.002 M HAuCl$_4$ solution then irradiated the mixture under a 100 W high-pressure mercury lamp for 1 h. The solution pH was controlled by adding 0.2 M NaCO$_3$. The UV–vis absorbance spectra demonstrated that Au nanoparticles enhanced the absorbance of Au/TiO$_2$ around near 563 nm. Hydrogen evolution performance by water splitting was improved more when using Au/TiO$_2$ as a photocatalyst than when adding pure TiO$_2$. Under UV irradiation, Au/TiO$_2$ produced about 35.04 μmol/g-cat of hydrogen, whereas pure TiO$_2$ produced a much smaller amount of hydrogen, about 0.79 μmol/g-cat. They also conducted a hydrogen evolution experiment under visible light only, although no hydrogen was
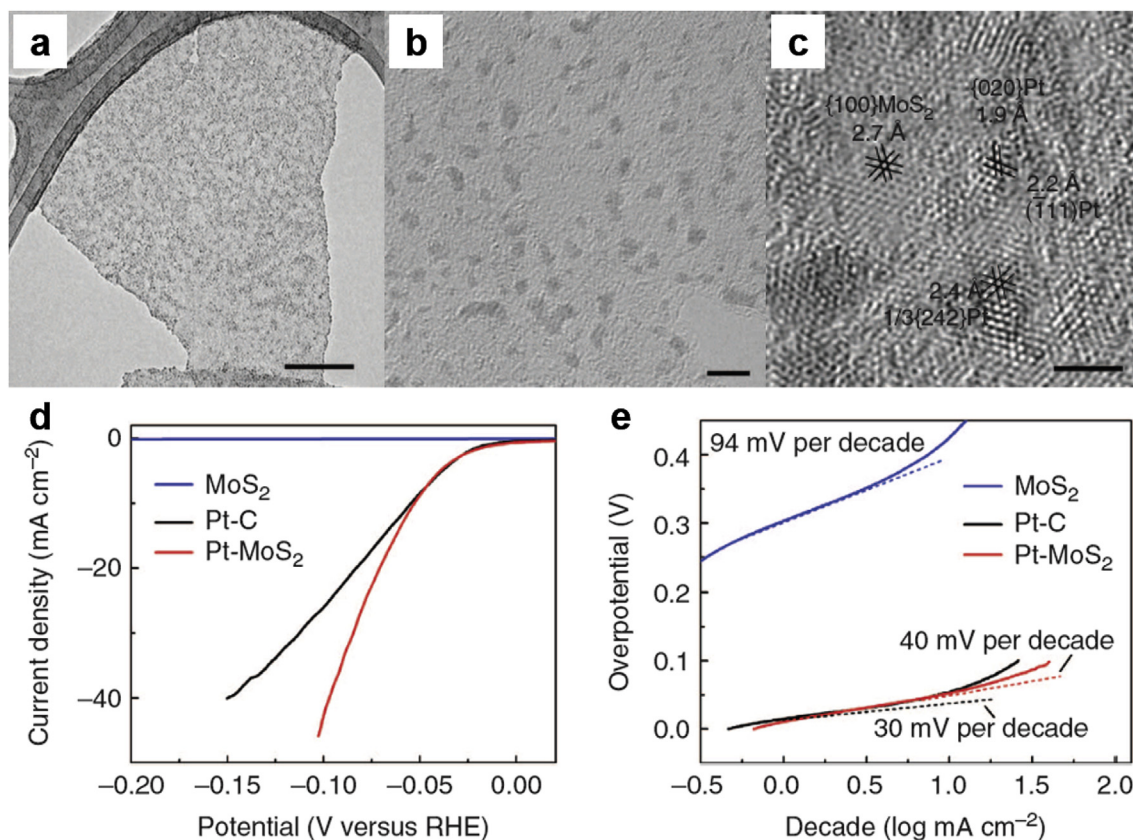

Fig. 4. (a) and (b) TEM images of Pt/MoS$_2$ nanosheet (scale bars are 100 nm and 5 nm, respectively). (c) HRTEM image of Pt/MoS$_2$ nanosheet with lattice fringes of Pt and MoS$_2$ (scale bar is 2 nm). (d) Polarization curves of Pt/MoS$_2$, Pt-C, and MoS$_2$. (e) Tafel plots of Pt/MoS$_2$, Pt-C, and MoS$_2$ [73].

detected. It was verified that the role of Au nanoparticles is to act as an electron sink, which disturbs the recombination of the electron-hole pair. They also offer active sites for catalytic reaction, whereas the surface plasmon resonance effect is not dominant.

For the HER study using TMDs, Huang et al. [73] synthesized Pt/MoS$_2$ hybrid nanomaterials by photodeposition method which reduced 0.2 mM K$_2$PtCl$_4$ solution to Pt nanoparticles on the MoS$_2$ nanosheets under a 150 W halogen lamp for 2 h in the presence of 0.3 mM trisodium citrate as a buffering agent. They then

investigated the catalytic activity of the Pt/MoS$_2$ nanocomposites for HER compared with commercial 10 wt% Pt on activated charcoal (Pt-C) catalysts and pure MoS$_2$. Fig. 4(a)-(c) show the TEM images of Pt/MoS$_2$ nanosheets; the size of the Pt nanoparticles is 1−3 nm. Fig. 4(d) and (e) show the HER performances of Pt/MoS$_2$, Pt-C, and pure MoS$_2$. Pt/MoS$_2$ and Pt-C improved the electrocatalytic activities of HER compared to pure MoS$_2$. In particular, Pt/MoS$_2$ exhibited the highest current density at the same potential. Also, the calculation showed that the Tafel slopes of Pt/MoS$_2$, Pt-C, and
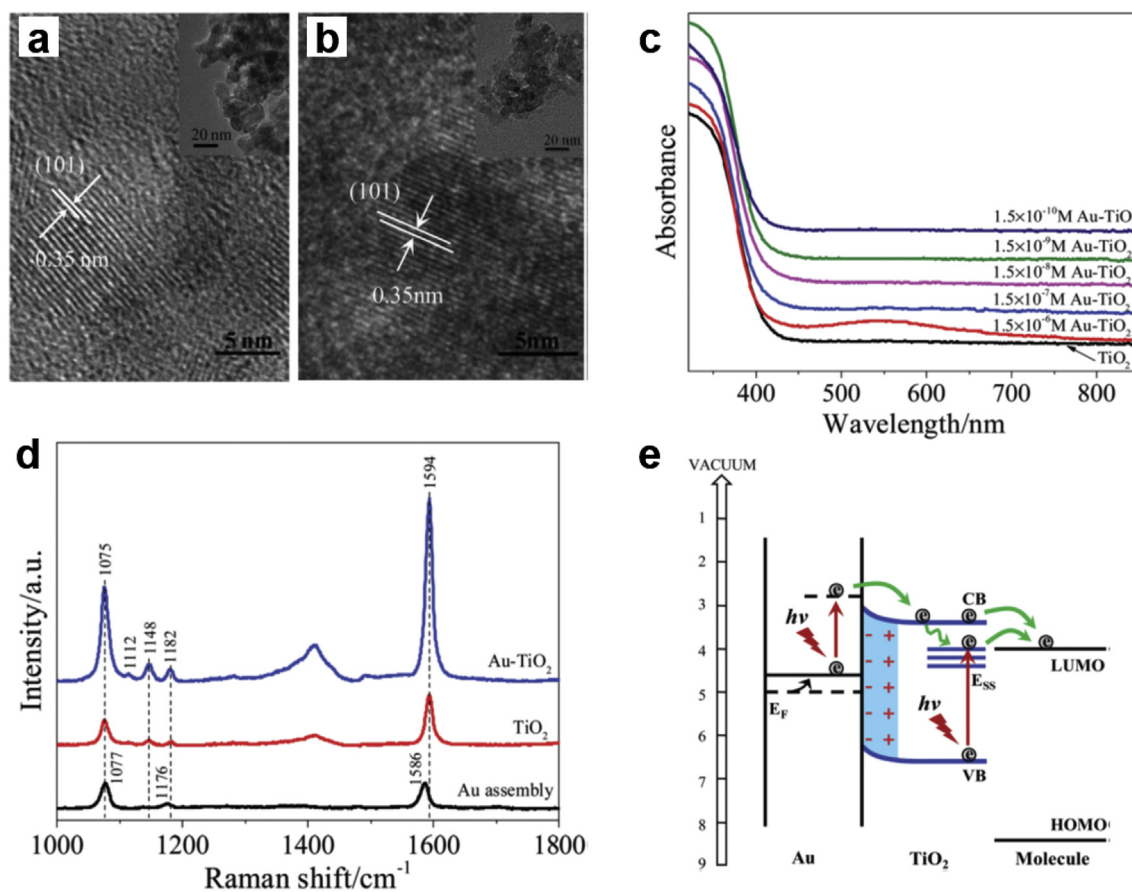

Fig. 5. (a) and (b) TEM images of pure TiO$_2$ and Au/TiO$_2$, respectively. (c) UV−vis diffuse reflectance spectra of TiO$_2$ and Au/TiO$_2$ nanocomposite with different amounts of Au. (d) SERS spectra of TiO$_2$, Au/TiO$_2$, and Au assembly substrate with 4-MBA adsorption. (e) Schematic diagram of SERS spectra enhancement [79].
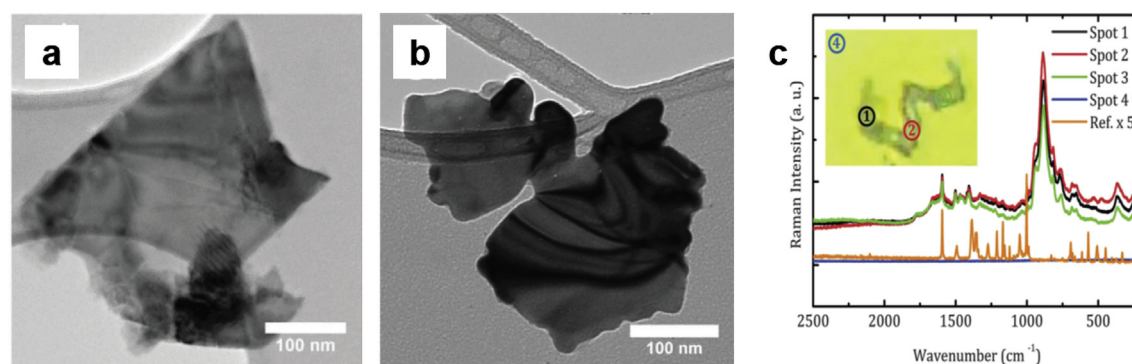

Fig. 6. TEM images of (a) pure MoS$_2$ flakes and (b) silver platelets after 90 + 45 min of illumination. (c) Raman spectra of PMT powder which adsorbed on the silver platelets. The inset displays an optical image of silver platelets and the numbers indicate the positions of the Raman measurement [80].

MoS_2 were 40, 30, and 94 mV dec^{-1}, respectively. These results reveal that the catalytic activity of Pt/MoS_2 hybrid nanomaterials has both Volmer-Tafel mechanisms and Volmer-Heyrovsky mechanisms. Zeng et al. [74] attempted to synthesize Pt/TiS_2 and Pt/TaS_2 by photodeposition method and measured the HER performance. They deposited Pt nanoparticles on the TiS_2 and TaS_2 by reducing 0.2 mM K_2PtCl_4 solution under a 150 W halogen lamp in the presence of 0.3 mM trisodium citrate. The electrocatalytic activities of Pt/TiS_2 and Pt/TaS_2 catalysts for HER exhibit excellent performance, in contrast to that of the pure TiS_2 and TaS_2, respectively. In particular, Pt/TiS_2 presented a Tafel slope of 40.6 V dec^{-1}, which was considerably lower than that of pure TiS_2 (102.5 V dec^{-1}) and was very close to that of commercial Pt-C (34.4 V dec^{-1}). Also, they investigated the stability of Pt/TiS_2 and Pt/TaS_2 catalysts after 1000 cycles, and demonstrated that these catalysts have good stability. Zhang et al. [75] also studied Pt loaded two-dimensional WS_2 nanosheets as an electrocatalyst for HER. They used the photodeposition method similar to that in the previous studies, and irradiated the WS_2 nanosheets under a 150 W halogen lamp for 2 h in the presence of 0.2 mM K_2PtCl_4 and 0.3 mM trisodium citrate. They also examined HER performance, which demonstrated that the Tafel slopes of Pt/WS_2 were 55 mV dec^{-1}. This result showed a higher slope than that of commercial Pt-C, the slope of which was 40 mV dec^{-1}, whereas it was lower than that of pure WS_2, the slope of which was 100 mV dec^{-1}.

3.3. Surface enhanced Raman scattering (SERS)

Surface enhanced Raman scattering (SERS) has been studied as one of the most effective analytical techniques related to the enhancement effect of a substrate [76–78]. Recently, SERS studies have focused on a metal/semiconductor based substrate, particularly using wide band gap semiconductors such as TMOs and TMDs. Metal/semiconductor based SERS substrates are expected to show more high-efficient performance due to the electromagnetic enhancement generated by the metal and due to the charge-transfer enhancement by the semiconductor [76,79].

For the study of SERS-active substrates, Jiang et al. [79] synthesized Au/TiO_2 nanocomposites with different amounts of Au by photodeposition method. They used a different concentration of $HAuCl_4$ solutions as a metal precursor (1.5 μM, 150 nM, 15 nM, 1.5 nM, and 0.15 nM) to deposit different amounts of Au under UV light irradiation. Fig. 5(a) and (b) show the TEM images of TiO_2 and Au/TiO_2 nanocomposites which have the same crystal lattice fringe as that of the anatase TiO_2. Fig. 5(c) and (d) show the UV–vis diffuse reflectance spectra and SERS spectra, respectively, of pure TiO_2 and Au/TiO_2 nanocomposites. UV–vis spectra of pure TiO_2 clearly shows absorptions in the range below 410 nm, which is consistent with the band gap of TiO_2 of about 3.2 eV. On the other hand, the Au/TiO_2 nanocomposites absorbed the range of 410–800 nm, which indicates the localized surface plasmon resonance absorption of Au. SERS spectra of 4-Mercaptobenzoic acid (4-MBA) on pure TiO_2, Au/TiO_2, and Au assembly substrates were measured. The results demonstrated the SERS enhancement of 4-MBA on Au/TiO_2 substrate due to the charge-transfer-induced enhancement of TiO_2 by the deposition of Au, as shown in Fig. 5(e).

To develop a SERS substrate using TMDs, Daeneke et al. [80] deposited silver on MoS_2 to fabricate a silver platelet for SERS substrate. MoS_2 nanosheets were prepared using the grinding assisted ultrasonic exfoliation method. Then, 10 mM $AgNO_3$ solution was added and irradiated under a 150 W Xe lamp for 90 min. After 90 min, large sized agglomerates were removed by centrifugation and the suspension was then illuminated for 45 min. Finally,

silver platelets were formed. Fig. 6(a) and (b) show TEM images of a MoS_2 flake and silver platelet after 90 + 45 min of illumination. Fig. 6(c) shows the Raman spectra of 1-phenyl-5-mercaptotetrazole (PMT) adsorbed on the silver platelets, which is located on the gold
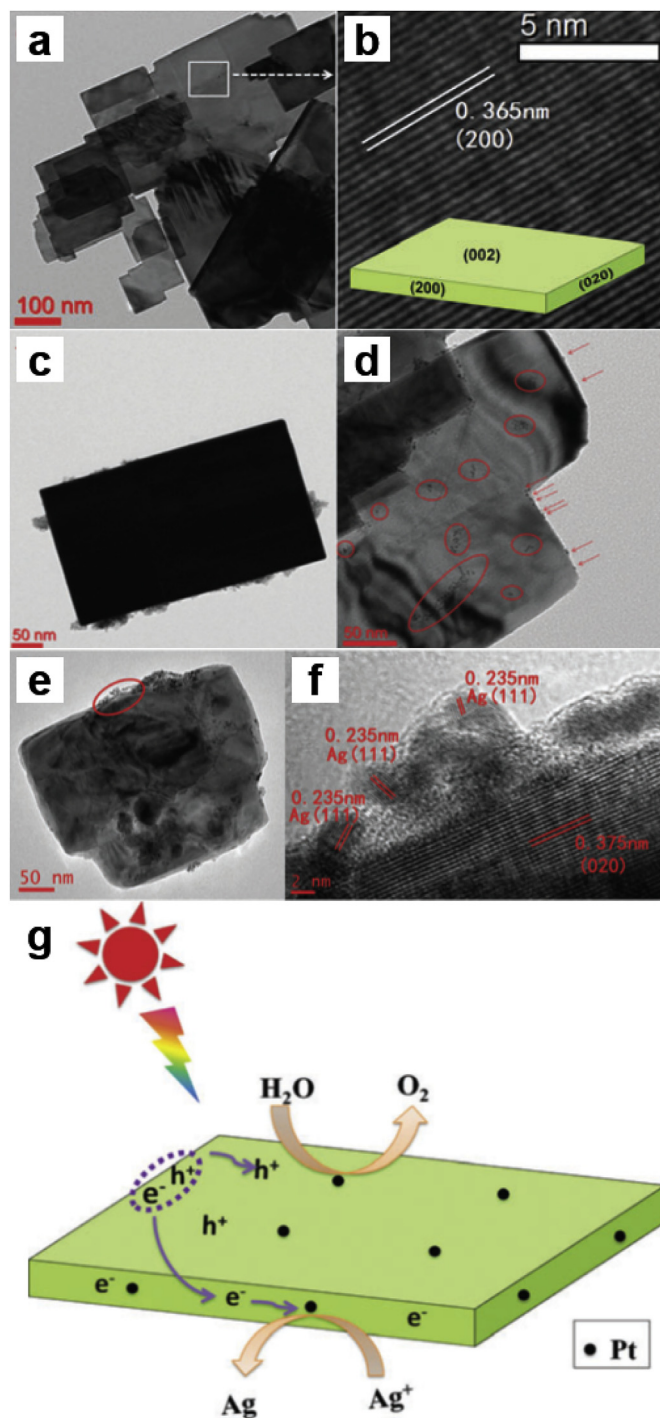

Fig. 7. (a) and (b) TEM and HRTEM images of square-like WO_3, respectively. The inset is a schematic diagram of square-like WO_3. (c) TEM image of Pt/WO_3 synthesized by photodeposition method. (d) TEM image of Pt/WO_3 synthesized by the ethylene glycol reduction process. (e) and (f) TEM and HRTEM images, respectively, of Pt/WO_3 synthesized by the ethylene glycol reduction process after irradiation 0.5 h with $AgNO_3$ solution. (g) Schematic diagram of photocatalytic water splitting O_2 evolution using Pt/WO_3 photocatalyst synthesized by the ethylene glycol reduction process [83].

coated wafer. Due to the SERS effect, the count rates of Raman mode at 367 cm^{-1} increased overall by a factor of 10 compared to pure PMT powder. Similarly, Lei et al. [81] also studied the growth of silver nanoparticles on MoS$_2$ flakes with lasers of different wavelengths (514.5, 633, and 785 nm) and performed a SERS investigation. They insisted that if the appropriate wavelength of the laser was irradiated, the role of MoS$_2$ is not only a photocatalyst but also offers surface defect sites induced by laser irradiation where Ag ion can be easily reduced. For SERS study, the Raman spectra of Rhodamine 6G (R6G) were measured. Compared to pure MoS$_2$ flake, R6G on Ag/MoS$_2$ substrate exhibited a strong intensity of Raman signal with a SERS enhancement factor of ~3 × 10^6.

3.4. Other applications

Guin et al. [82] reported the antibacterial activity of Ag/TiO$_2$ nanoparticles/nanotubes. They used dried TiO$_2$ nanoparticles/nanotubes and polyvinyl alcohol (PVA)-capped colloidal TiO$_2$ nanoparticles/nanotubes. Ag nanoparticles were deposited on TiO$_2$ nanoparticles/nanotubes by reducing AgNO$_3$ solution to Ag under a 365 nm of 400 W UV light for 5 h. Antibacterial activity was demonstrated by standard disc diffusion method. PVA-capped colloidal Ag-TiO$_2$ nanoparticles exhibited the highest antibacterial activity against *Escherichia coli*, since the Ag nanoparticles were well distributed on the PVA.

Gong et al. [83] demonstrated the spatial charge separation of square-like WO$_3$ nanoplates along the crystal facets through photodeposition method. As shown in Fig. 7(a) and (b), square-like WO$_3$ nanoplates showed the predominant (002) facet and the minor (200) and (020) facets. Fig. 7(c) and (d) show TEM images of the Pt/WO$_3$ nanoplates which were prepared by reducing H$_2$PtCl$_6$ using the photodeposition method and the ethylene glycol reduction process, respectively. The images show that the Pt nanoparticles were deposited on the minor (002) and (200) facets of square-like WO$_3$ nanoplates when using the photodeposition method. However, they were deposited on both the predominant (002) facet and the minor (020) and (200) facets when using the ethylene glycol reduction process. Fig. 7(e) and (f) show the TEM and HRTEM images, respectively, of Pt/WO$_3$ nanoplates synthesized by ethylene glycol reduction process after irradiation for 0.5 h in the presence of AgNO$_3$ solution. Ag nanoparticles were obviously deposited on the edge facets corresponding to the result of the deposition of Pt nanoparticles by the photodeposition method. These results verified that the light-induced charge separation of square-like WO$_3$ nanoplates photogenerated the electrons and holes toward the minor and major facets respectively, as shown in Fig. 7(g).

For an electrical application, He et al. [84] performed a study of Pt/MoS$_2$ thin-film transistor (TFT) arrays for a NO$_2$ gas sensor. MoS$_2$ was prepared by electrochemical lithiation, which exhibited p-type behavior, and the reduced graphene oxide (rGO) was used as an electrode. Pt nanoparticles were deposited on the MoS$_2$ surface by photodeposition method. 0.2 mM K$_2$PtCl$_4$ and 0.3 mM sodium citrate were used as a metal precursor and buffer agent, respectively, and were irradiated under a 150 W halogen lamp for 12 h. Fig. 8(a) shows the response of the MoS$_2$, rGO, Pt/MoS$_2$, and Pt/rGO TFT sensor arrays under NO$_2$ exposure. Sensitivity was calculated as $(I_1 - I_0)/I_0 \times 100\%$, where I_0 and I_1 were currents of the device at initial NO$_2$ exposure and after NO$_2$ exposure. Fig. 8(b) indicates that Pt/MoS$_2$ TFT arrays exhibit ~3 times higher sensitivity than other TFT sensor arrays. Since a Schottky junction between MoS$_2$ and Pt was formed and NO$_2$ could adsorb at the interface of Pt and MoS$_2$, the sensitivity was increased.

Qiao et al. [85] studied noble metal loaded MoS$_2$ for the catalytic reduction of *p*-nitrophenol (p-NP) to *p*-aminophenol (p-AP). They prepared Ag, Au, Pd, and Pt loaded MoS$_2$ nanosheets by reducing metal precursors such as AgNO$_3$, HAuCl$_4$·3H$_2$O, K$_2$PdCl$_6$, and H$_2$PtCl$_6$·6H$_2$O under UV light irradiation. As shown in Fig. 9(a)-(h), noble metal nanoparticles were uniformly formed on the surface of the MoS$_2$ nanosheets, since MoS$_2$ nanosheets have defective sites where metal ions can be anchored by electrostatic interaction. Noble metal/MoS$_2$ nanocomposites exhibited the catalytic activity for the reduction of p-NP to p-AP in the presence of NaBH$_4$. In the reduction process, p-NP is ionized to p-NP ions in the presence of NaBH$_4$, and is then reduced to p-AP by catalytic activity. Each step of the p-NP to p-AP reduction process was verified by UV−vis absorbance spectra shifting, as shown in Fig. 9(i)-(k), and the entire process was completed within 12 min. This reduction process can be considered a pseudo-first-order reaction since, during the process, the concentration of NaBH$_4$ is not significantly affected due to its high initial concentration compared to p-NP. Thus, this reaction can be written as

$$\ln(C_t/C_0) = \kappa_{app} \cdot t$$

where C_t and C_0 are the concentrations of p-NP at time t and 0, respectively, and κ_{app} is the apparent rate constant (min^{-1}). In this manner, the catalytic activities of MoS$_2$ and noble metal (Ag, Au, Pd, and Pt) loaded MoS$_2$ can be the plot of $\ln(C_t/C_0)$ versus time, as shown in Fig. 9(l). Among these catalytic activities, it is clearly demonstrated that Pd/MoS$_2$ nanosheets catalyst exhibited the highest catalytic performance, which is 2.5 times higher than the pure MoS$_2$ nanosheets catalyst. The mechanism of noble metal loaded MoS$_2$ nanosheets catalyst involves the transfer of electrons from BH$_4^-$ anions to MoS$_2$ and then to the noble metal, which causes the reduction of p-NP to p-AP, as shown in Fig. 9(m).
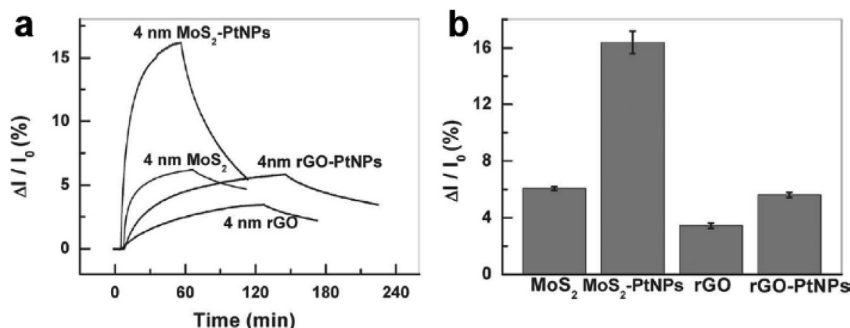

Fig. 8. (a) Response of different TFT sensors with exposure of 1.2 ppm NO$_2$ gas. (b) Sensitivity of different TFT sensors [84].
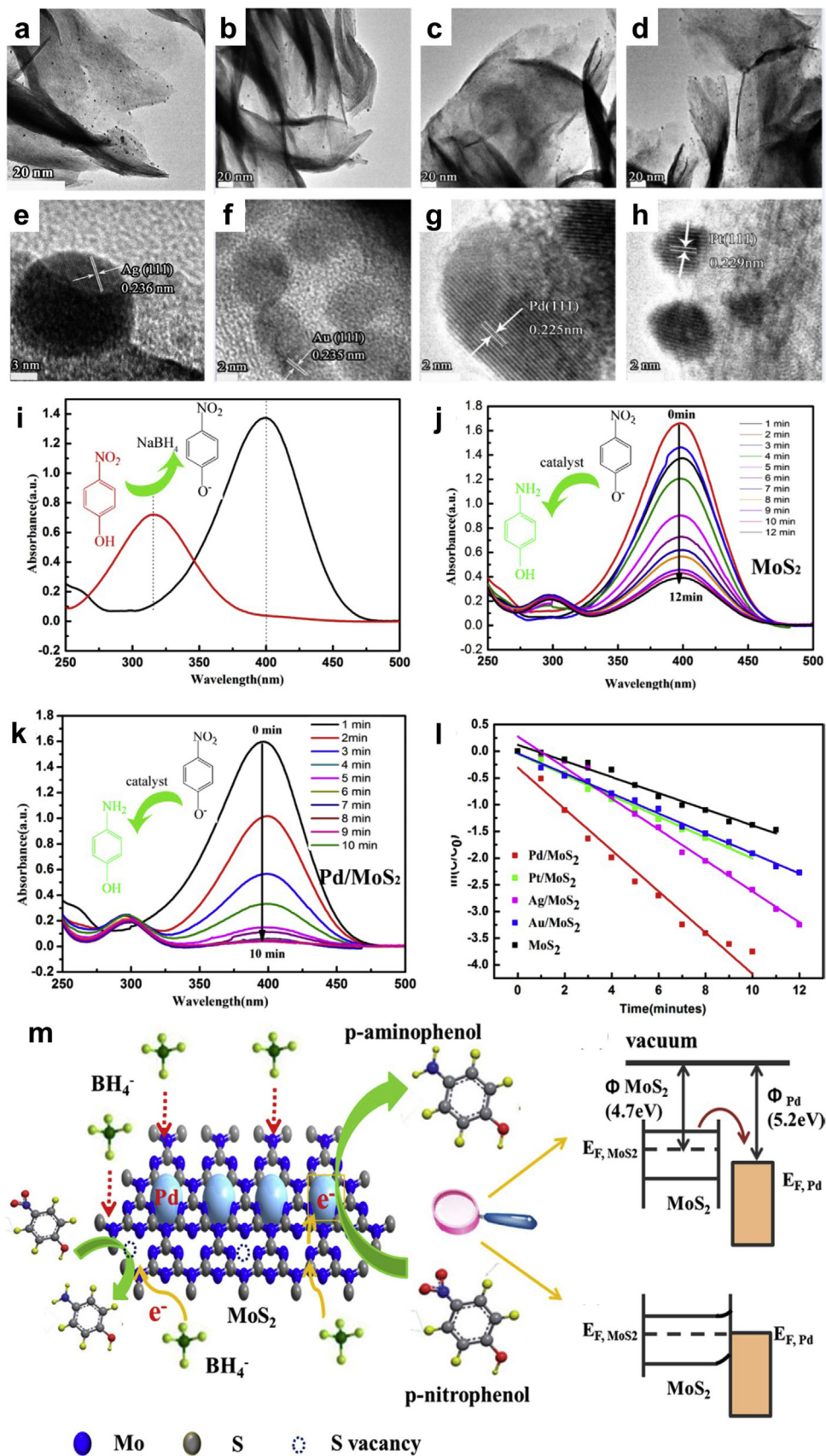
Fig. 9. (a)–(d) TEM and (d)–(f) HRTEM images of Ag/MoS$_2$ (a and e), Au/MoS$_2$ (b and f), Pd/MoS$_2$ (c and g), and Pt/MoS$_2$ (d and h). (i)–(k) UV–vis spectra during catalytic reduction process from p-NP to p-AP. (m) Schematic diagram of catalytic reduction process [85].

Table 1
List of nanocomposites prepared by photodeposition and their applications.

Semiconductor		Metal	Metal precursor	Light source	Application	Ref
TMO	TiO_2	Pt	H_2PtCl_6	Xe lamp	Photocatalytic water splitting	[61]
	TiO_2	Pt	H_2PtCl_6	UV lamp	Photocatalytic reduction of CO_2 to Methane	[62]
	TiO_2	Pt	H_2PtCl_6	Mercury lamp	Visible light photocatalyst	[63]
	TiO_2	Pd	Na_2PdCl_4	Sunlight	Visible light photocatalyst	[64]
	TiO_2	Pd	$Pd(NO_3)_2$	UV lamp	Photocatalysis	[65]
	ZnO	Au	$HAuCl_4$	Xe lamp	Photocatalytic water splitting	[66]
	TiO_2	Au	$HAuCl_4$	Mercury lamp	HER	[72]
	TiO_2	Au	$HAuCl_4$	UV lamp	SERS	[79]
	TiO_2	Ag	$AgNO_3$	UV lamp	Antibacterial activity	[82]
	WO_3	Pt	H_2PtCl_6	Xe lamp	Facet engineering	[83]
TMD	MoS_2	Pt	K_2PtCl_4	Halogen lamp	HER	[73]
	TiS_2, TaS_2	Pt	K_2PtCl_4	Halogen lamp	HER	[74]
	WS_2	Pt	K_2PtCl_4	Halogen lamp	HER	[75]
	MoS_2	Ag	$AgNO_3$	Xe lamp	SERS	[80]
	MoS_2	Ag	$AgNO_3$	Laser (514.5, 633, 785 nm)	SERS	[81]
	MoS_2	Pt	K_2PtCl_4	Halogen lamp	NO_2 gas sensor	[84]
	MoS_2	Ag	$AgNO_3$	Mercury lamp	Catalytic reduction of *p*-nitrophenol	[85]
		Au	$HAuCl_4$			
		Pd	K_2PdCl_6			
		Pt	H_2PtCl_6			

4. Conclusion

In summary, as shown in Table 1, transition metal oxides and dichalcogenides have been widely studied for various applications such as photocatalyst, HER, SERS, etc. However, since the use of individual components has limitations, nanocomposites have been developed using a variety of synthesis methods. Among these methods, we focused on transition metal oxides and dichalcogenides decorated with noble metal nanoparticles prepared by the photodeposition method and their applications. Metal nanoparticles can be grown on the surface of TMOs and TMDs under light exposure, and the amount of metal nanoparticles is easily controlled by changing the concentration of the metal solution or light exposure time and power. As mentioned above, the semiconductor in the photodeposition method acts as (i) a template for metal nanoparticles and (ii) photocatalytic reaction. A number of other researchers insisted that light-induced defect sites of semiconductors act as nucleation for metal growth. In the view of performance, metal nanoparticles (i) provide active sites for reaction and (ii) act as electron acceptors which tune the band gap of the semiconductor. Furthermore, in optical applications, metal nanoparticles also have the important role of providing a surface plasmon resonance effect; however, this mainly depends on the size of the metal nanoparticles. The number of decorated metal nanoparticles can affect the performance of nanocomposites, since overloaded metal nanoparticles can include electron scattering sites or block the light which decreases the performance. For further applications based on nanocomposite materials, the photodeposition method has the potential for synthesis of nanocomposites. However, challenges remain in defining and optimizing the parameters of the photodeposition method.

References

[1] Chen H, Wang L. Nanostructure sensitization of transition metal oxides for visible-light photocatalysis. Beilstein J Nanotechnol 2014;5:696−710.

[2] Guo T, Yao M-S, Lin Y-H, Nan C-W. A comprehensive review on synthesis methods for transition-metal oxide nanostructures. CrystEngComm 2015;17:3551−85.

[3] Xu M, Liang T, Shi M, Chen H. Graphene-like two-dimensional materials. Chem Rev 2013;113:3766−98.

[4] Sun Y, Gao S, Xie Y. Atomically-thick two-dimensional crystals: electronic structure regulation and energy device construction. Chem Soc Rev 2014;43:530−46.

[5] Bhimanapati GR, Lin Z, Meunier V, Jung Y, Cha J, Das S, et al. Recent advances in two-dimensional materials beyond graphene. ACS Nano 2015;9:11509−39.

[6] Geim AK, Novoselov KS. The rise of graphene. Nat Mater 2007;6:183−91.

[7] Choi W, Lahiri I, Seelaboyina R, Kang YS. Synthesis of graphene and its applications: a review. Crit Rev Solid State Mater Sci 2010;35:52−71.

[8] Neto AHC, Novoselov K. New directions in science and technology: two-dimensional crystals. Rep Prog Phys 2011;74, 082501.

[9] Yin Y, Alivisatos AP. Colloidal nanocrystal synthesis and the organic-inorganic interface. Nature 2005;437:664−70.

[10] Cozzoli PD, Pellegrino T, Manna L. Synthesis, properties and perspectives of hybrid nanocrystal structures. Chem Soc Rev 2006;35:1195−208.

[11] Camargo PHC, Satyanarayana KG, Wypych F. Nanocomposites: synthesis, structure, properties and new application opportunities. Mater Res-Ibero-Am J 2009;12:1−39.

[12] Mann S. Self-assembly and transformation of hybrid nano-objects and nanostructures under equilibrium and non-equilibrium conditions. Nat Mater 2009;8:781−92.

[13] Costi R, Saunders AE, Banin U. Colloidal hybrid nanostructures: a new type of functional materials. Angew Chem Int Ed Engl 2010;49:4878−97.

[14] Du AJ, Ng YH, Bell NJ, Zhu ZH, Amal R, Smith SC. Hybrid graphene/titania nanocomposite: interface charge transfer, hole doping, and sensitization for visible light response. J Phys Chem Lett 2011;2:894−9.

[15] Huang X, Qi X, Boey F, Zhang H. Graphene-based composites. Chem Soc Rev 2012;41:666−86.

[16] Xiang QJ, Yu JG, Jaroniec M. Graphene-based semiconductor photocatalysts. Chem Soc Rev 2012;41:782−96.

[17] Zhang N, Liu SQ, Xu YJ. Recent progress on metal core@semiconductor shell nanocomposites as a promising type of photocatalyst. Nanoscale 2012;4:2227−38.

[18] Huang X, Tan C, Yin Z, Zhang H. 25th anniversary article: hybrid nanostructures based on two-dimensional nanomaterials. Adv Mater 2014;26:2185−204.

[19] Wang H, Zhang L, Chen Z, Hu J, Li S, Wang Z, et al. Semiconductor hetero-junction photocatalysts: design, construction, and photocatalytic perfor-mances. Chem Soc Rev 2014;43:5234—44.

[20] Sun M, Liu H, Liu Y, Qu J, Li J. Graphene-based transition metal oxide nano-composites for the oxygen reduction reaction. Nanoscale 2015;7:1250—69.

[21] Tan C, Zhang H. Two-dimensional transition metal dichalcogenide nanosheet-based composites. Chem Soc Rev 2015;44:2713—31.

[22] Xie XQ, Kretschmer K, Wang GX. Advances in graphene-based semiconductor photocatalysts for solar energy conversion: fundamentals and materials en-gineering. Nanoscale 2015;7:13278—92.

[23] Fan WQ, Zhang QH, Wang Y. Semiconductor-based nanocomposites for photocatalytic H-2 production and CO2 conversion. Phys Chem Chem Phys 2013;15:2632—49.

[24] Lin J, Li H, Zhang H, Chen W. Plasmonic enhancement of photocurrent in MoS2 field-effect-transistor. Appl Phys Lett 2013;102:203109.

[25] Chen CH, Wu CL, Pu J, Chiu MH, Kumar P, Takenobu T, et al. Hole mobility enhancement and p-doping in monolayer WSe2 by gold decoration. 2d Mater 2014;1.

[26] Bhanu U, Islam MR, Tetard L, Khondaker SI. Photoluminescence quenching in gold - MoS2 hybrid nanoflakes. Sci Rep-Uk 2014;4.

[27] Miao JS, Hu WD, Jing YL, Luo WJ, Liao L, Pan AL, et al. Surface plasmon-enhanced photodetection in few layer MoS2 phototransistors with Au nano-structure arrays. Small 2015;11:2392—8.

[28] Wu XF, Song HY, Yoon JM, Yu YT, Chen YF. Synthesis of core-shell Au@TiO2 nanoparticles with truncated wedge-shaped morphology and their photo-catalytic properties. Langmuir 2009;25:6438—47.

[29] Kmetyko A, Mogyorosi K, Gerse V, Konya Z, Pusztai P, Dombi A, et al. Pho-tocatalytic H(2) production using Pt-TiO(2) in the presence of oxalic acid: influence of the noble metal size and the carrier gas flow rate. Materials (Basel) 2014;7:7022—38.

[30] Fu S, He Y, Wu Q, Wu Y, Wu T. Visible-light responsive plasmonic Ag2O/Ag/g-C3N4 nanosheets with enhanced photocatalytic degradation of Rhodamine B. J Mater Res 2016;31:2252—60.

[31] Chen K, Ma L, Wang J-H, Cheng Z-Q, Yang D-J, Li Y-Y, et al. Integrating metallic nanoparticles of Au and Pt with MoS2—CdS hybrids for high-efficient photo-catalytic hydrogen generation via plasmon-induced electron and energy transfer. RSC Adv 2017;7:26097—103.

[32] Kim YG, Jo W-K. Photodeposited-metal/CdS/ZnO heterostructures for solar photocatalytic hydrogen production under different conditions. Int J Hydrogen Energy 2017;42:11356—63.

[33] Marschall R, Wang L. Non-metal doping of transition metal oxides for visible-light photocatalysis. Catal Today 2014;225:111—35.

[34] Kalantar-zadeh K, Ou JZ, Daeneke T, Mitchell A, Sasaki T, Fuhrer MS. Two dimensional and layered transition metal oxides. Appl Mater Today 2016;5: 73—89.

[35] Momeni MM, Ghayeb Y. Photoinduced deposition of gold nanoparticles on TiO2—WO3 nanotube films as efficient photoanodes for solar water splitting. Appl Phys A 2016;122.

[36] Lee SC, Lintang HO, Yuliati L. High photocatalytic activity of Fe2O3/TiO2 nanocomposites prepared by photodeposition for degradation of 2,4-dichlorophenoxyacetic acid. Beilstein J Nanotechnol 2017;8:915—26.

[37] Singhal N, Kumar U. Noble metal modified TiO 2 : selective photoreduction of CO 2 to hydrocarbons. Molecular Catalysis 2017;439:91—9.

[38] Wang QH, Kalantar-Zadeh K, Kis A, Coleman JN, Strano MS. Electronics and optoelectronics of two-dimensional transition metal dichalcogenides. Nat Nanotechnol 2012;7:699—712.

[39] Chhowalla M, Shin HS, Eda G, Li LJ, Loh KP, Zhang H. The chemistry of two-dimensional layered transition metal dichalcogenide nanosheets. Nat Chem 2013;5:263—75.

[40] Ganatra R, Zhang Q. Few-Layer MoS2: a promising layered semiconductor. ACS Nano 2014;8:4074—99.

[41] Li H, Wu J, Yin Z, Zhang H. Preparation and applications of mechanically exfoliated single-layer and multilayer MoS(2) and WSe(2) nanosheets. Acc Chem Res 2014;47:1067—75.

[42] He Z, Que W. Molybdenum disulfide nanomaterials: structures, properties, synthesis and recent progress on hydrogen evolution reaction. Appl Mater Today 2016;3:23—56.

[43] Peng W, Li Y, Zhang F, Zhang G, Fan X. Roles of two-dimensional transition metal dichalcogenides as cocatalysts in photocatalytic hydrogen evolution and environmental remediation. Ind Eng Chem Res 2017;56:4611—26.

[44] Kumar SG, Devi LG. Review on modified TiO2 photocatalysis under UV/visible light: selected results and related mechanisms on interfacial charge carrier transfer dynamics. J Phys Chem 2011;115:13211—41.

[45] Zhao S, Huang J, Huo Q, Zhou X, Tu W. A non-noble metal MoS2—Cd0.5Zn0.5S photocatalyst with efficient activity for high H2evolution under visible light irradiation. J Mater Chem 2016;4:193—9.

[46] Li J, Zeng HC. Size tuning, functionalization, and reactivation of Au in TiO2 nanoreactors. Angew Chem 2005;117:4416—9.

[47] Zhang N, Liu S, Fu X, Xu Y-J. Synthesis of M@TiO2(m = Au, Pd, Pt) core—shell nanocomposites with tunable photoreactivity. J Phys Chem C 2011;115: 9136—45.

[48] Perera SD, Mariano RG, Vu K, Nour N, Seitz O, Chabal Y, et al. Hydrothermal synthesis of graphene-TiO2 nanotube composites with enhanced photo-catalytic activity. ACS Catal 2012;2:949—56.

[49] Shi YM, Huang JK, Jin LM, Hsu YT, Yu SF, Li LJ, et al. Selective decoration of Au

[50] Liu Y, Yu YX, Zhang WD. MoS2/CdS heterojunction with high photo-electrochemical activity for H-2 evolution under visible light: the role of MoS2. J Phys Chem C 2013;117:12949—57.

[51] Zhou J, Zhao Y, Bao J, Huo D, Fa H, Shen X, et al. One-step electrodeposition of Au-Pt bimetallic nanoparticles on MoS 2 nanoflowers for hydrogen peroxide enzyme-free electrochemical sensor. Electrochim Acta 2017;250:152—8.

[52] Kim J, Byun S, Smith AJ, Yu J, Huang J. Enhanced electrocatalytic properties of transition-metal dichalcogenides sheets by spontaneous gold nanoparticle decoration. J Phys Chem Lett 2013;4:1227—32.

[53] Sarkar D, Xie X, Kang J, Zhang H, Liu W, Navarrete J, et al. Functionalization of transition metal dichalcogenides with metallic nanoparticles: implications for doping and gas-sensing. Nano Lett 2015;15:2852—62.

[54] Cao J, Zhang X, Zhang Y, Zhou J, Chen Y, Liu X. Free MoS2 nanoflowers grown on graphene by microwave-assisted synthesis as highly efficient non-noble-metal electrocatalysts for the hydrogen evolution reaction. PLoS One 2016;11, e0161374.

[55] Singha SS, Nandi D, Bhattacharya TS, Mondal PK, Singha A. Photoluminescence modulation due to conversion of trions to excitons and plasmonic interaction in MoS 2 -metal NPs hybrid structures. J Alloy Comp 2017;723:722—8.

[56] Zhao L, Chen X, Wang X, Zhang Y, Wei W, Sun Y, et al. One-step solvothermal synthesis of a carbon@TiO(2) dyade structure effectively promoting visible-light photocatalysis. Adv Mater 2010;22:3317—21.

[57] Chenthamarakshan CR, Ming Y, Rajeshwar K. Underpotential photocatalytic deposition: a new preparative route to composite semiconductors. Chem Mater 2000;12. 3538-+.

[58] Wenderich K, Mul G. Methods, mechanism, and applications of photo-deposition in photocatalysis: a review. Chem Rev 2016;116:14587—619.

[59] Luo B, Liu G, Wang L. Recent advances in 2D materials for photocatalysis. Nanoscale 2016;8:6904—20.

[60] Zhou N, López-Puente V, Wang Q, Polavarapu L, Pastoriza-Santos I, Xu Q-H. Plasmon-enhanced light harvesting: applications in enhanced photocatalysis, photodynamic therapy and photovoltaics. RSC Adv 2015;5:29076—97.

[61] Yu JG, Qi LF, Jaroniec M. Hydrogen production by photocatalytic water split-ting over Pt/TiO2 nanosheets with exposed (001) facets. J Phys Chem C 2010;114:13118—25.

[62] Li QY, Zong LL, Li C, Cao YH, Wang XD, Yang JJ. Photocatalytic reduction of CO2 to methane on Pt/TiO2 nanosheet porous film. Adv Condens Matter Phys 2014;2014:1—6.

[63] Lv J, Gao HZ, Wang HG, Lu XJ, Xu GQ, Wang DM, et al. Controlled deposition and enhanced visible light photocatalytic performance of Pt-modified TiO2 nanotube arrays. Appl Surf Sci 2015;351:225—31.

[64] Leong KH, Chu HY, Ibrahim S, Saravanan P. Palladium nanoparticles anchored to anatase TiO2 for enhanced surface plasmon resonance-stimulated, visible-light-driven photocatalytic activity. Beilstein J Nanotechnol 2015;6:428—37.

[65] Khojasteh H, Salavati-Niasari M, Abbasi A, Azizi F, Enhessari M. Synthesis, characterization and photocatalytic activity of PdO/TiO2 and Pd/TiO2 nano-composites. J Mater Sci-Mater El 2016;27:1261—9.

[66] Wang T, Lv R, Zhang P, Li CJ, Gong JL. Au nanoparticle sensitized ZnO nano-pencil arrays for photoelectrochemical water splitting. Nanoscale 2015;7: 77—81.

[67] Zeng M, Li Y. Recent advances in heterogeneous electrocatalysts for the hydrogen evolution reaction. J Mater Chem 2015;3:14942—62.

[68] Fan W, Lai Q, Zhang Q, Wang Y. Nanocomposites of TiO2and reduced gra-phene oxide as efficient photocatalysts for hydrogen evolution. J Phys Chem C 2011;115:10694—701.

[69] Benck JD, Hellstern TR, Kibsgaard J, Chakthranont P, Jaramillo TF. Catalyzing the hydrogen evolution reaction (HER) with molybdenum sulfide nano-materials. ACS Catal 2014;4:3957—71.

[70] Cheng L, Huang W, Gong Q, Liu C, Liu Z, Li Y, et al. Ultrathin WS2 nanoflakes as a high-performance electrocatalyst for the hydrogen evolution reaction. Angew Chem Int Ed Engl. 2014;53:7860—3.

[71] Vesborg PC, Seger B, Chorkendorff I. Recent development in hydrogen evo-lution reaction catalysts and their practical implementation. J Phys Chem Lett 2015;6:951—7.

[72] Chen JJ, Wu JCS, Wu PC, Tsai DP. Plasmonic photocatalyst for H-2 evolution in photocatalytic water splitting. J Phys Chem C 2011;115:210—6.

[73] Huang X, Zeng Z, Bao S, Wang M, Qi X, Fan Z, et al. Solution-phase epitaxial growth of noble metal nanostructures on dispersible single-layer molybde-num disulfide nanosheets. Mol Ther 2013;4:1444.

[74] Zeng Z, Tan C, Huang X, Bao S, Zhang H. Growth of noble metal nanoparticles on single-layer TiS2and TaS2nanosheets for hydrogen evolution reaction. Energy Environ Sci 2014;7:797—803.

[75] Zhang YX, Yan JQ, Ren XP, Pang LQ, Chen H, Liu S. 2D WS2 nanosheet sup-ported Pt nanoparticles for enhanced hydrogen evolution reaction. Int J Hydrogen Energy 2017;42:5472—7.

[76] Fateixa S, Nogueira HI, Trindade T. Hybrid nanostructures for SERS: materials development and chemical detection. Phys Chem Chem Phys 2015;17: 21046—71.

[77] Wang AX, Kong X. Review of recent progress of plasmonic materials and nano-structures for surface-enhanced Raman scattering. Materials (Basel) 2015;8:3024—52.

[78] Mosier-Boss PA. Review of SERS substrates for chemical sensing. Nano-materials (Basel) 2017;7.

[79] Jiang X, Sun XD, Yin D, Li XL, Yang M, Han XX, et al. Recyclable Au-TiO2

nanocomposite SERS-active substrates contributed by synergistic charge-transfer effect. Phys Chem Chem Phys 2017;19:11212—9.

[80] Daeneke T, Carey BJ, Chrimes AF, Ou JZ, Lau DWM, Gibson BC, et al. Light driven growth of silver nanoplatelets on 2D MoS2 nanosheet templates. J Mater Chem C 2015;3:4771—8.

[81] Lei YT, Li DW, Zhang TC, Huang X, Liu L, Lu YF. One-step selective formation of silver nanoparticles on atomic layered MoS2 by laser-induced defect engineering and photoreduction. J Mater Chem C 2017;5:8883—92.

[82] Guin D, Manorama SV, Latha JNL, Singh S. Photoreduction of silver on bare and colloidal TiO2 Nanoparticles/Nanotubes: synthesis, characterization, and tested for antibacterial outcome. J Phys Chem C 2007;111:13393—7.

[83] Gong HH, Ma RR, Mao F, Liu KW, Cao HM, Yan HJ. Light-induced spatial separation of charges toward different crystal facets of square-like WO3. Chem Commun 2016;52:11979—82.

[84] He Q, Zeng Z, Yin Z, Li H, Wu S, Huang X, et al. Fabrication of flexible MoS2 thin-film transistor arrays for practical gas-sensing applications. Small 2012;8:2994—9.

[85] Qiao X-Q, Zhang Z-W, Tian F-Y, Hou D-F, Tian Z-F, Li D-S, et al. Enhanced catalytic reduction of p-nitrophenol on ultrathin MoS2 nanosheets decorated with noble metal nanoparticles. Cryst Growth Des 2017;17:3538—47.

Dr. Jangho Kim is an Assistant Professor of Biosystems Engineering at Chonnam National University. Prior to joining the current position, he studied as a Senior Researcher of the Research Institute for Agriculture and Life Sciences, Seoul National University. He also studied as a Research Scholar in the Thin Film & Charged Particles Research Laboratory at Department of Electrical and Computer Engineering, University of Illinois. His research interests include 1) micro/nanofabrication & biologically inspired engineering systems, 2) mechanobiology & tissue engineering, and 3) bio-nanotechnology. He has authored and co-authored more than 80 peer-reviewed journal publications and 8 issued patent in the area of biomaterials and tissue engineering focused on the nano/microtechnology. Among the awards he has received are Young Scientist Award (Korean and Japan Society for Biomaterials, 2012), Young Plenary Speaker (TERMIS-AP conference, 2013), Samsung HumanTech Paper Award (Samsung Electronics, 2014), Keynote Speaker (TERM STEM 2014), and Promising Young Scientist (Korean Society of Mechanical Engineers 2016).
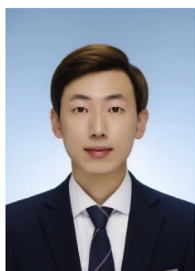
Yoonkyung Lee is a MS/Ph.D. student in the School of Mechanical Engineering at Sungkyunkwan University. He has dual B.S. degrees in Biomechatronics and Mechanical Engineering respectively from Sungkyunkwan University in 2017. His main research interests are focused on the properties of two-dimensional nanomaterials and materials processing.

Dr. WonHyoung Ryu is an Associate Professor of Department of Mechanical Engineering at YONSEI University, Seoul in Republic of Korea. He received a B.S. degree in Mechanical Engineering from Seoul National University, M.S. degrees in Aeronautics/Astronautics and Manufacturing Systems Engineering from Stanford University, and a Ph.D. degree in Mechanical Engineering from Stanford University. His research interests are in advanced nano and micro fabrication technologies for biomedical devices and bio solar energy systems. He serves as an associate editor of Journal of Mechanical Science and Technology and an editorial board member of International Journal of Precision Engineering and Manufacturing-Green Technology.

Eunpa Kim is a senior engineer at Samsung Electronics. Prior to this, he was a postdoctoral fellow at the University of California, Berkeley. He received his PhD degree in mechanical engineering from the University of California, Berkeley, in 2014. Kim's research interests include micro-/nanoscale fabrication and nanometrology of low-dimensional semiconducting nanomaterial.

Junsuk Rho is the principal investigator of Nanoscale Photonics and Integrated Manufacturing Laboratory and an assistant professor in the Department of Mechanical Engineering and the Department of Chemical Engineering at POSTECH, Korea. He received his B.S., M.S., Ph.D. in Mechanical Engineering at Seoul National University, University of Illinois, Urbana-Champaign, University of California, Berkeley, respectively. His research focuses on the fundamental studies of deep sub-wavelength nanophotonics and their applications to sub-wavelength imaging, cavities, and photonic devices.

Yunjeong Park received her B.S. in Mechanical engineering from Sungkyunkwan University in 2017. She is a first year Ph.D. student in the School of Mechanical Engineering at Sungkyunkwan University. Her primary research includes two-dimensional bionanoelectronics and design of hybrid bionanostructures.

Dr. Kyunghoon Kim is an Assistant Professor in the School of Mechanical Engineering at Sungkyunkwan University. He received his B.S. in Mechanical Engineering from Sungkyunkwan University. After he received a M.S. degree in the Department of Mechanical Engineering from Stanford University, he worked as a senior engineer for Samsung Electronics, where his main research project was focused on strategic analysis for fuel cell business feasibility and design of fuel cell system. He holds a Ph.D. in Mechanical Engineering from UC Berkeley. His primary research interests are bio/nano engineering; bionanoelectronics, biomimetic nanostructures, and mechanical behavior and laser processing of materials.